Modelling the Arabian Sea with a 1/2°-resolution ROMS model

May 2019

Carolyne Chercham

Report written as part of the course
Modélisation 3D (OPB205)

Within the framework of an Erasmus+ exchange,
involving the two following Master programs:

Sciences de la Mer, Aix-Marseille Université
Ocean and Climate physics, Universität Hamburg

Summer semester 2019

Abstract

The Arabian Sea, located in the northern Indian Ocean, is strongly impacted by the Monsoon cycle. The Monsoon winds originate in large-scale atmospheric pressure differences between land and sea. Over the Arabian Sea, Monsoon winds are southwesterly winds during summer time and northeasterly winds during winter. The influence of the Monsoon cycle on the western Arabian Sea is investigated with a Regional Ocean Modelling System (ROMS) numerical model. The model is climatologically forced and has a spatial resolution of 1/2°. The seasonally varying surface circulation and the coastal upwelling and downwelling processes are represented in the model.

La Mer d'Arabie, située dans l'Océan Indien Nord, est fortement impactée par le cycle des Moussons. Les vents des Moussons ont leur origine dans des différences de pression atmosphérique de grandes échelles entre la terre et la mer. Au-dessus de la Mer d'Arabie, les vents des Moussons sont des vents du sud-ouest durant l'été et des vents du nord-est pendant l'hiver. L'influence du cycle des Moussons sur la Mer d'Arabie occidentale est étudiée avec un modèle numérique Regional Ocean Modelling System (ROMS). Le forçage du modèle est climatologique et la résolution spatiale du modèle est de 1/2°. La circulation de surface qui varie avec les saisons, ainsi que l'upwelling et le downwelling côtier sont bien représentés dans le modèle.

1 Introduction

The Arabian Sea is located in the northern Indian Ocean, between the Arabian Peninsula and the Indian subcontinent. It is well known for its seasonal circulation reversal which is connected to the Monsoon wind cycle. The monsoon winds change in direction due to the differentiated heating and cooling of the Asian landmasses in winter and summer compared to the Sea Surface Temperature (SST) of the adjacent watermasses. The resulting low and high pressure systems and in particular the pressure gradient lead to the monsoon winds. While the land is characterized by low pressure during summer, it is characterized by high pressure during winter time. Taking into account the Coriolis force and other processes, the resulting prevailing winds over the Arabian Sea are southwesterly winds during summer time (southwest monsoon, SWM) and northeasterly winds during winter time (northeast monsoon, NEM).
The circulation in the Arabian Sea is affected by those steady winds, notably in the Western part of the Arabian Sea, where the SWM and NEM winds are alongshore winds. Upwelling or downwelling therefore occur at the coast of the Arabian Peninsula, depending on the season. Moreover, the Arabian Sea exhibits some seasonally recurring eddies, which are the subject of numerical investigations (e.g. Luther and O'Brien, 1985; Vic et al., 2014).
Numerical modelling of atmospheric and ocean dynamics appeared during the last century and evolved from Richardson's 1922 dream of the human "Forecast factory" towards general circulation models (GCMs), of which some are even run on so-called supercomputers (Doglioli, 2016). The Regional Ocean Modelling System (ROMS) is an example of an ocean GCM. It is supported by a strong community (`http://www.myroms.org/`) and comes with a number of tools to simplify its usage.

The purpose of this work is to run a 1/2°-resolution ROMS model with a basic configuration and climatological forcing for the region of the Arabian Sea and to compare results with observational and other model data. A special focus is set on the western Arabian Sea.

2 Methods and data

This section introduces the ROMS model in general and the specificities of the 1/2°-resolution model executed for the Arabian Sea region.

2.1 ROMS: Regional Ocean Modeling System

ROMS is a 3D ocean model based on the numerical resolution of Boussinesq approximated horizontal momentum equations (Eq. 1 & 2), hydrostatic vertical momentum balance (Eq. 3), mass conservation (Eq. 4), heat and freshwater conservation equations (Eq. 5 & 6), as well as the equation of state (Eq. 7) (Shchepetkin and McWilliams, 2005; Doglioli, 2016):

$$\frac{\partial u}{\partial t} + u \cdot \nabla u - fv = -\frac{1}{\rho_0}\frac{\partial P}{\partial x} + A_h \nabla_h^2 u + A_v \frac{\partial^2 u}{\partial z^2} \tag{1}$$

$$\frac{\partial v}{\partial t} + u \cdot \nabla u + fu = -\frac{1}{\rho_0}\frac{\partial P}{\partial y} + A_h \nabla_h^2 v + A_v \frac{\partial^2 v}{\partial z^2} \tag{2}$$

$$0 = \frac{\partial P}{\partial z} + \rho g \tag{3}$$

$$0 = \frac{\partial u}{\partial x} + \frac{\partial v}{\partial y} + \frac{\partial w}{\partial z} \tag{4}$$

$$\frac{\partial T}{\partial t} + u \cdot \nabla T = K_h \nabla_h^2 T + K_v \frac{\partial^2 T}{\partial z^2} \quad (5)$$

$$\frac{\partial S}{\partial t} + u \cdot \nabla S = K_h \nabla_h^2 S + K_v \frac{\partial^2 S}{\partial z^2} \quad (6)$$

$$\rho = \rho(T, S, z) \quad (7)$$

where u and v are the meridional and zonal velocity components (m.s^{-1}), w the vertical velocity component (m.s^{-1}), t the time (s), f the Coriolis parameter (s^{-1}), ρ the density and ρ_0 the reference density (kg.m^{-3}), P the pressure (Pa), x and y the meridional and zonal space coordinates (m), z the upward oriented vertical coordinate (m), A_h and A_v the horizontal and vertical viscosity coefficients (m^2.s^{-1}), g the gravity of Earth (m.s^{-2}), T the temperature (°C), S the salinity, K_h and K_v the horizontal and vertical diffusivity coefficients (m^2.s^{-1}).

ROMS differentiates between baroclinic and barotropic modes, and therefore requires an outer (smaller) and an inner (larger) time step. The previous equations are solved for every inner time step. Meanwhile, the following shallow water equations are solved for every outer time step:

$$\frac{\partial U}{\partial t} + U\frac{\partial U}{\partial x} + V\frac{\partial U}{\partial y} = -g\frac{\partial \eta}{\partial x} + fV + A_h\left(\frac{\partial^2 U}{\partial x^2} + \frac{\partial^2 U}{\partial y^2}\right) + F_x + B_x$$

$$\frac{\partial V}{\partial t} + U\frac{\partial V}{\partial x} + V\frac{\partial V}{\partial y} = -g\frac{\partial \eta}{\partial y} - fU + A_h\left(\frac{\partial^2 V}{\partial x^2} + \frac{\partial^2 V}{\partial y^2}\right) + F_y + B_y$$

$$\frac{\partial \eta}{\partial t} + \frac{\partial (HU)}{\partial x} + \frac{\partial (HU)}{\partial y} = 0\,, \qquad with \quad H = h + \eta$$

where U, V are barotropic velocities (m.s^{-1}), η the surface elevation (m), F_x the wind forcing (m.s^{-2}), B_x the bottom friction (m.s^{-2}), H the total water height (m) and h the water height below $z = 0$ m (m).

All of the previous equations are solved on a staggered two-dimensional horizontal grid, which is known as Arakawa C-grid (1977) illustrated in Fig. 1. The variables are positioned at different locations on that grid and therefore offset from one each other.

In the vertical, ROMS uses terrain-following curvilinear coordinates which permit higher resolution of surface and bottom boundary layers. Vertical mixing processes are parameterized with the K-profile parameterization (KPP) after Large et al. (1994).

The French Institut de Recherche pour le Développement (IRD) made use of the Adaptive Grid Refinement in Fortran (AGRIF) to create ROMS_AGRIF in which several different grids can be nested Penven et al. (2006). IRD also released ROMSTOOLS, a useful toolbox for the setup of the model domain and for the analysis of results. ROMS_AGRIF and ROMSTOOLS (Penven et al., 2008) are provided by `https://www.croco-ocean.org`.

2.2 Climatological 1/2°-resolution ROMS model of the Arabian Sea

Using ROMS_AGRIF version 3.1.1, a climatological 1/2°-resolution model of the Arabian Sea was run on the OSU Pythéas cluster for an integration period of 10 years.
More specifications on the bathymetry and domain, the grid and time steps, the forcing and the initial conditions are given in the following.

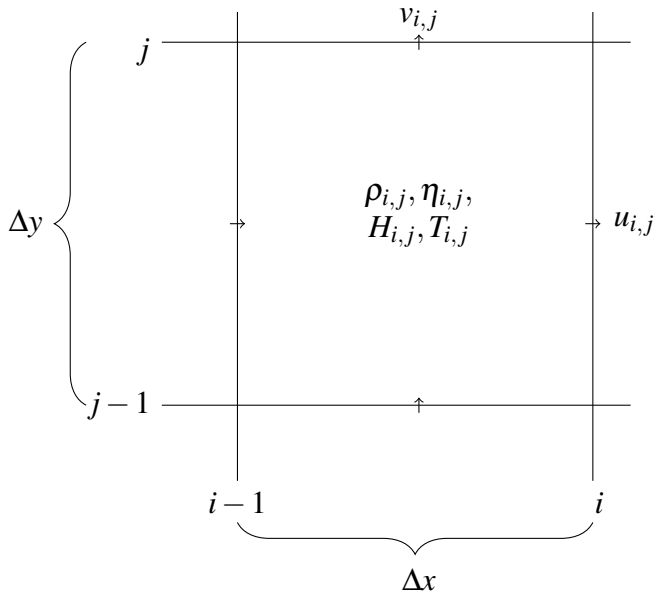

Figure 1 – Schematic of location of variables on the Arakawa C-grid. i, j are the zonal and meridional indices, $\Delta x, \Delta y$ indicate the grid spacing. u, v are the zonal and meridional velocities. ρ is the density, η the surface elevation, H the water depth and T the temperature.

2.2.1 Bathymetry and domain

The model domain extends from 8°N to 28°N, and from 51°E to 78°E (Fig. 2). The bathymetry (ETOPO2) and coastline data (GSHHS) used are publicly available datasets (see `http://www.croco-ocean.org/download/datasets/`). The Persian Gulf and the Gulf of Oman are masked as 'land' using the preprocessing `make_grid` tool.

The southern and western boundaries are indicated as open. The northern and eastern boundaries are closed.

2.2.2 Grid and time steps

To keep the integration time short, the grid spacing is chosen to be 1/2°. Therefore `LLm0 = 53` and `MMm0 = 42`. The number of vertical levels is set to `N = 32`.

The outer (`NDTFAST`) and inner (`dt`) time steps are chosen in order to respect the Courant-Friedrichs-Lewy (CFL) criterion for their mode:

$$\Delta t \leq \frac{1}{c}\left(\frac{1}{\Delta x^2}+\frac{1}{\Delta y^2}\right)^{-\frac{1}{2}}$$

where Δt is the time step, Δx and Δy the spatial steps, and c the propagation velocity of the considered waves.
The time steps are therefore chosen as:
`NDTFAST` = 60 s; `dt` = 3600 s.

A year in this 10-year run consists of 12 months with 30 days of 86400 s each. A restart file (`NRST` = 720) and 10 3-day-averaged output files (`NAVG` = 72) are saved for every month.

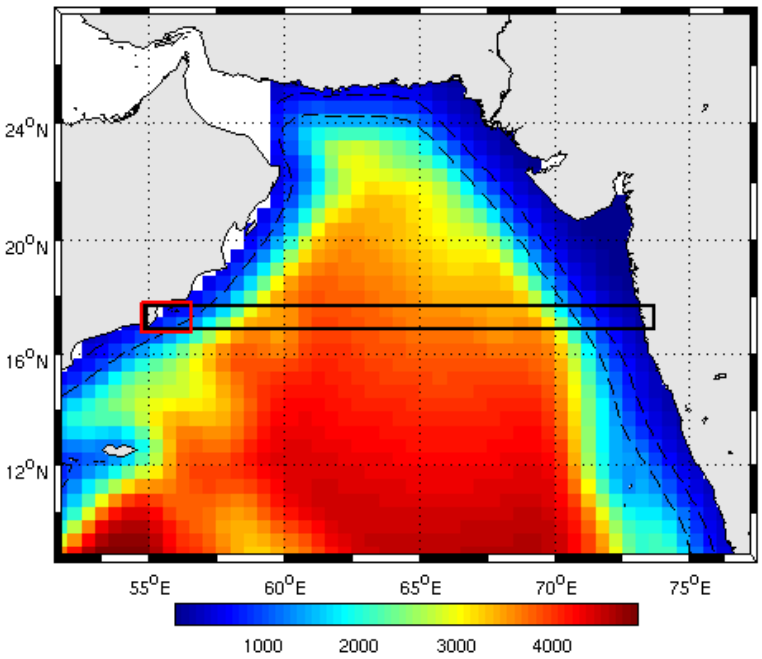

Figure 2 – Bathymetry (m) of the model domain (8°N – 28°N, 51°E – 78°E) centered on the Arabian Sea. Note that the Persian Gulf and Gulf of Oman were masked as 'land' when selecting the model domain with ROMSTOOLS. The black rectangle indicates the region of the Arabian Sea at approximately 17.5°N used for the Hovmöller diagrams in Fig. 5 and the red rectangle indicates the zone at 17°N, 56°E used for the depiction of wind stress in Fig. 5(a) and of vertical velocity profiles in Fig. 6.

2.2.3 Climatological forcing and initial conditions

Surface forcing parameters such as wind stress or short wave radiation are obtained from the Comprehensive Ocean-Atmosphere Data Set (COADS05) and stored in the `roms_frc.nc` file. The forcing data is data with 12 entries (a climatological year) which is interpolated between the months.
Initial and open boundary conditions are computed from World Ocean Atlas Data (WOA2009) using the thermal wind equations (Doglioli, 2016), and stored in the `roms_ini.nc` file and the `roms_clm.nc` file.

3 Results

Using the MATLAB tools provided by ROMSTOOLS, the overall diagnostics of the run were computed and are shown in Fig. 3. All seven depicted statistical variables (volume anomaly, surface averaged kinetic energy, as well as volume averaged kinetic energy, diffusion, vertical velocities, salinity and temperature) undergo seasonal variations which reflect the seasonality of the applied forcing. The surface averaged kinetic energy is highest in summer, and so is the the volume averaged kinetic energy. The volume anomaly experiences more intraannual variations, with several local maxima and minima. The peak is reached in late spring and the absolute minimum occurs in autumn of each year.
Moreover, these diagnostics show that the first two years of the run can be considered its spin-up period, where especially the volume averaged diffusion (diff3d) depicts that the model has not yet reached a stable state. Discarding the first two years, most of the statistical variables

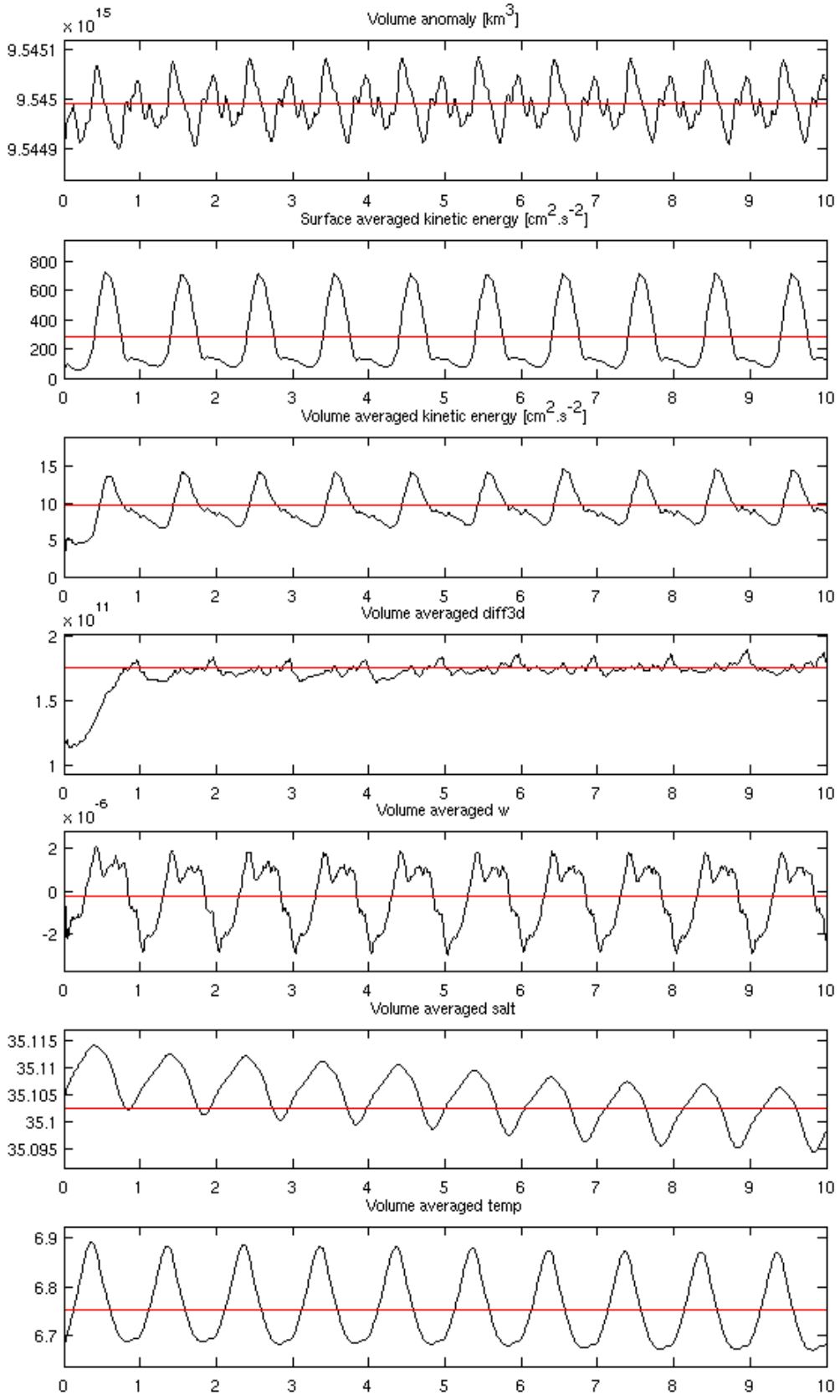

Figure 3 – Diagnostics of the 10-year Arabian Sea run, calculated with ROMSTOOLS. From top to bottom: Volume anomaly (km^3); surface averaged kinetic energy ($cm^2.s^{-2}$); volume averaged kinetic energy ($cm^2.s^{-2}$); volume averaged diffusion (diff3d); volume averaged w ($m.s^{-1}$); volume averaged salinity; volume averaged temperature (°C).

do not show trends. Thus the average total volume in the domain and the surface averaged kinetic energy stay constant. However, the volume averaged salinity and temperature show both a slight negative trend, which means that heat and salt are lost over time.
In the following, only the years 3 to 10 of the run are considered.

The surface circulation in the model domain varies with the season. During the SWM, the near-coast circulation is anti-cyclonic and the center of the model domain is characterised by strong eastward currents (Fig. 4). Between SWM and NEM, the surface circulation reverses. During the NEM, the near-coast circulation is cyclonic and the center of the model domain is characterised by meandering southwestward currents (not shown).

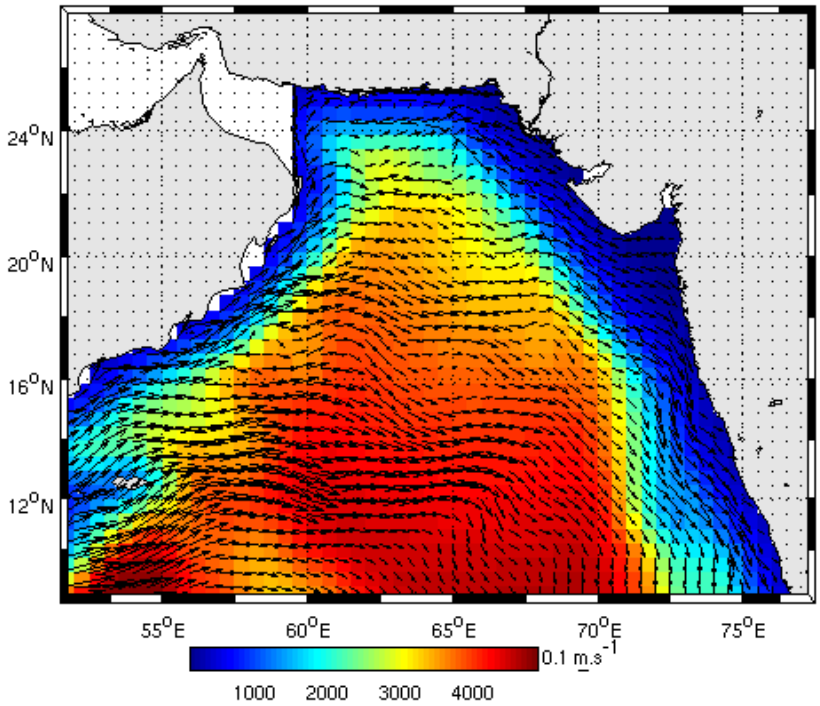

Figure 4 – 3-day averaged surface currents in the beginning of July of the tenth year of the Arabian Sea run. The colours indicate the bathymetry (m).

The surface wind stress at 17.5°N, 56°E (Fig 5(a)) is exemplary for the seasonal variation of wind stress forcing in the western Arabian Sea. The u-momentum and the v-momentum stress vary in the same way. The windstress therefore reflects the shift from northeasterly winds (negative values), prevailing from October to February, to southwesterly winds (positive values), prevailing from March to September. The maximum wind stress occurs in July, while its most negative value occurs in December. The magnitude of the summer maximum is three times larger than the magnitude of the winter minimum. The summer SWM is more intense than the winter NEM.
This seasonality of the wind stress magnitude and direction is not only reflected in the surface circulation of the whole Arabian Sea (see Fig. 4) but appears even better in the climatologically averaged surface u velocity component (Fig. 5(b)) along 17.5°N. From May to September, the surface u velocity component is positive across the whole Arabian Sea at that latitude. The highest values are found at the Western boundary, where they reach up to $0.5\,\mathrm{m.s^{-1}}$. During March and April the zonal velocity component at the western and eastern boundary are already

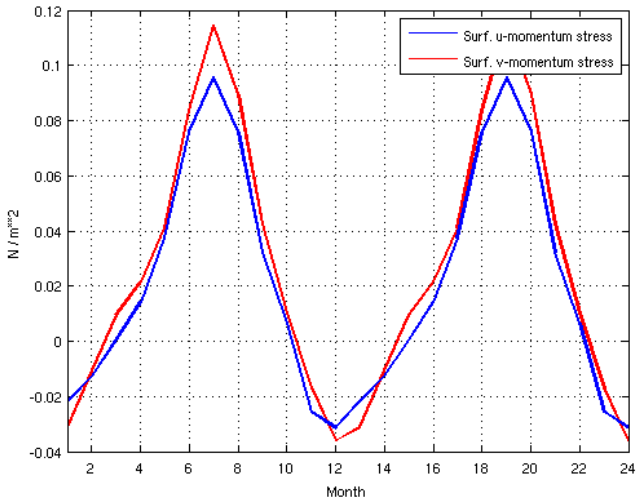

(a) Wind stress (N.m^{-2})

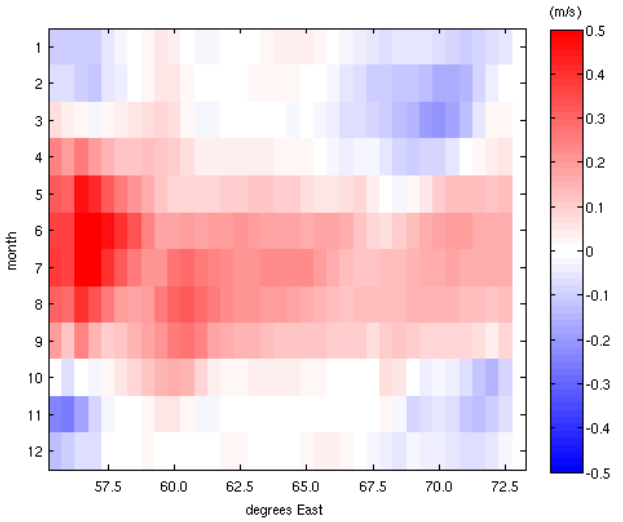

(b) u (m.s^{-1}) at surface

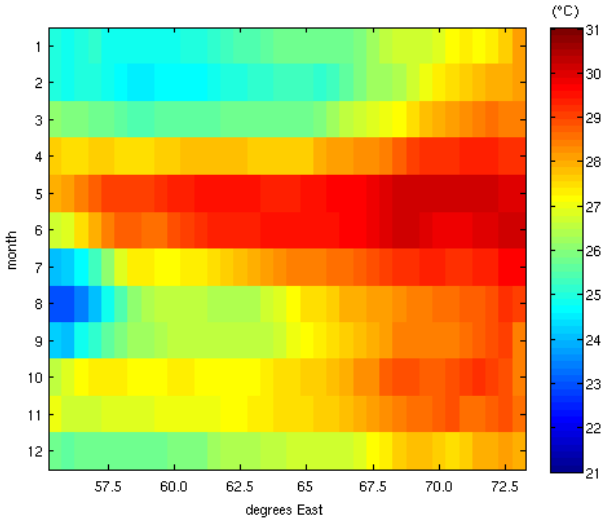

(c) SST (°C)

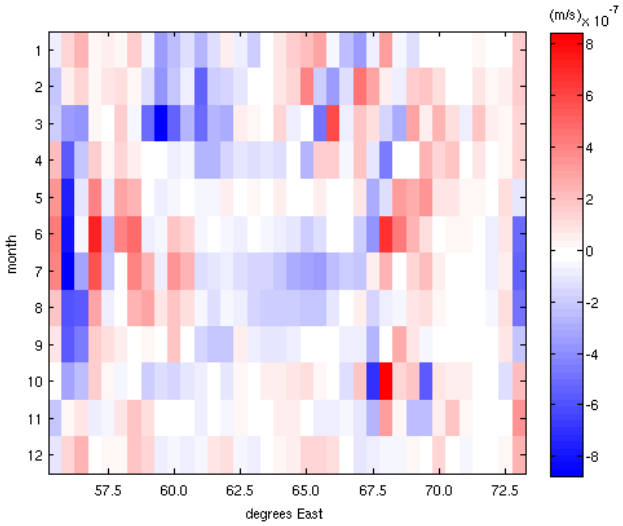

(d) w ($\times 10^{-7}$ m.s^{-1}) at surface

Figure 5 – Climatological wind stress forcing (17.5°N, 56°E) and climatological Hovmöller diagrams at approximately 17.5°N. (a) Climatological u (blue line) and v (red line) wind stress forcing depicted for two years in row. (b) Hovmöller diagram of climatologically averaged surface u velocity. (c) Hovmöller diagram of climatologically averaged SST. (d) Hovmöller diagram of climatologically averaged surface w velocity.

directed eastwards, while the zonal velocity between 65°E and 72°E is still oriented westwards. During the months of October to February, the zonal velocity at the western and eastern boundaries is either negative or zero, while it stays positive or zero between 57.5°E and 67.5°E.
The SST reflects vertical heat fluxes and radiation as well as advection (and diffusion). The climatological SST at 17.5°N (Fig. 5(c)) is highest at the eastern boundary during May and June, with temperatures up to 31°C. During these two months the SST is above 29°C everywhere at that latitude, except for the western boundary, where SST drops below 27°C in June. The absolute minimum in SST occurs in August at the western boundary, with temperatures slightly above 22°C, while the SST at the eastern boundary is close to 30°C at that time. Another local minimum occurs during winter, when SST falls as low as 24°C in the western part.
Climatological surface vertical velocities at 17.5°N (Fig. 5(d)) do not show a pattern which is as clear as the one for the zonal velocities. During all climatological months, both upward (positive) and downward (negative) velocities occur, depicting local upwelling and downwelling. However, from April to October, near the western boundary, upward velocities occur in the first grid cell (starting from the coast), while negative velocities occur in the two following grid cells, followed by one grid cell with positive values. Beyond that, the pattern becomes more complex. Downward velocities occur at the western coast during the winter months.

The near-surface vertical velocities in winter and summer in the first grid cell next to the western coast differ by their sign. They are directed downwards during winter and upwards during summer. Profiles of the 3-day averaged vertical velocity in the beginning of February and August (Fig. 6) show that the downwelling taking place during winter is smaller in magnitude than the upwelling taking place during summer. While the vertical velocity in the upper 100 m varies between -1$\times10^{-5}$ m.s^{-1} and 0$\times10^{-5}$ m.s^{-1} in February, it varies between -0.2$\times10^{-5}$ m.s^{-1} and 12.1$\times10^{-5}$ m.s^{-1} in August, with the maximum velocity being reached at 30 m depth.

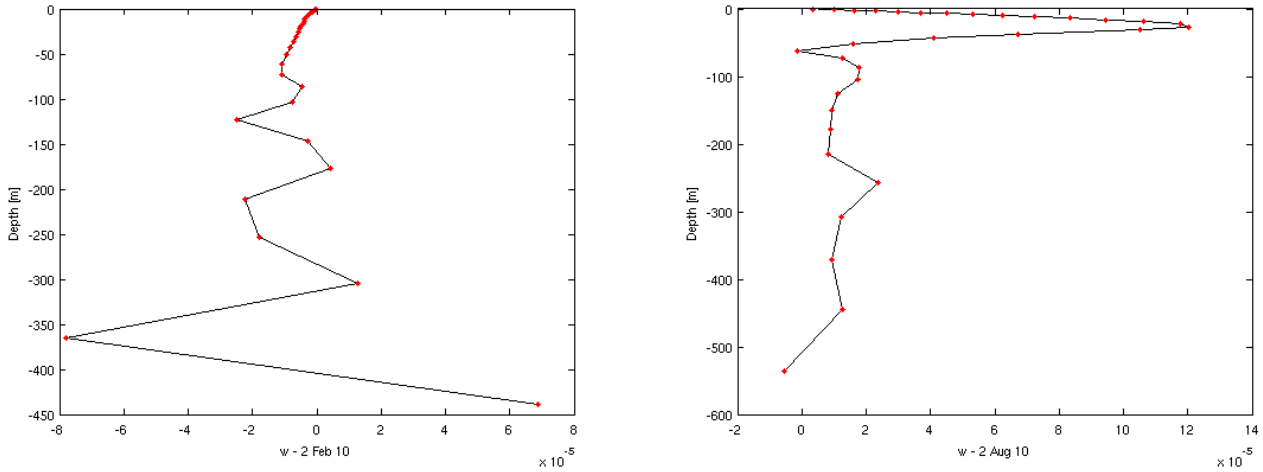

(a) w ($\times10^{-5}$ m.s^{-1}) in February

(b) w ($\times10^{-5}$ m.s^{-1}) in August

Figure 6 – 3-day averaged vertical velocity w in the beginning of February (a) and August (b) of the tenth year of the Arabian Sea run at approximately 17°N and 56°E. Note that neither vertical nor horizontal axes ranges are consistent between (a) and (b).

4 Discussion

The diagnostics indicate that the model has gained in stability after two years of spin-up. However, the volume averaged salinity and temperature show a slight negative trend.
Lee et al. (2000) observe high salinity and high temperature water being advected into the Arabian Sea from the Persian Gulf through the Gulf of Oman. Having masked out the Gulf of Oman and the Persian Gulf for the model domain might therefore be one reason for the negative trend observed in the volume averaged salinity and temperature of the diagnostics (Fig. 3).

The overall surface circulation of the Arabian Sea corresponds to observations and other model results. ADCP observations of along-shelf surface currents during SWM confirm that these are mostly oriented downwind at the western boundary (Lee et al., 2000). The general SWM surface circulation in the 1/2°-resolution ROMS (ROMS_AGRIF 3.1.1) model is comparable to the SWM surface circulation obtained by Vic et al. (2014) in a 1/16°-resolution ROMS (ROMS_AGRIF 3.0) model with the same climatological atmospheric forcing (Fig. 7). The coastal currents in the northern Arabian Sea are anti-cyclonic and there is eastward currents in the center between the Arabian Peninsula and India. Data from surface drifter climatology indicates similar circulation patterns (Lumpkin and Johnson, 2013; Vic et al., 2014).

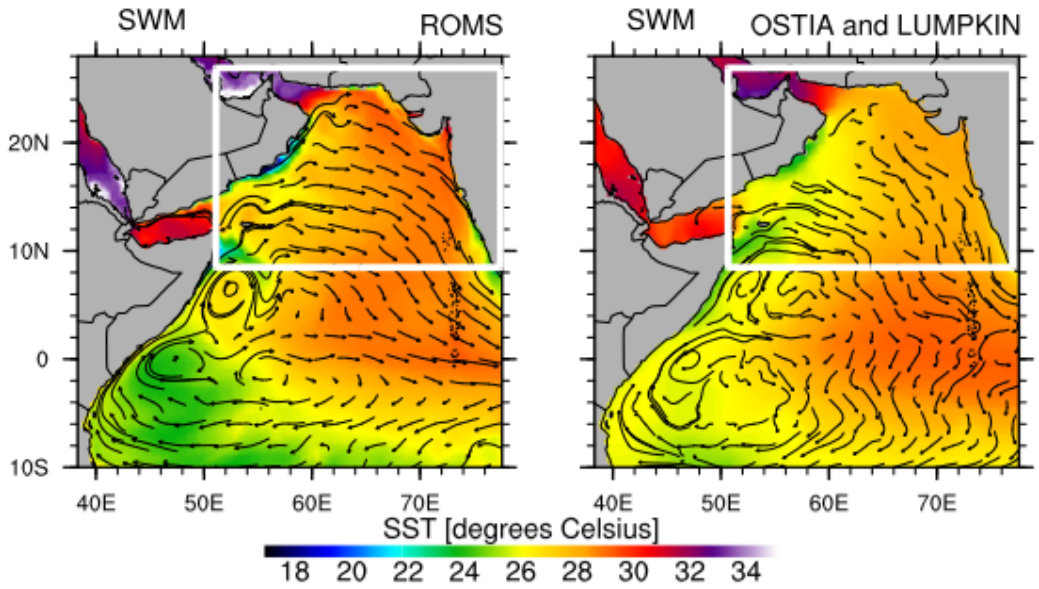

Figure 7 – Climatology of surface circulation an SST in the Arabian Sea during SWM. Data on the left originate from 10-year 1/16°-resolution ROMS model by Vic et al. (2014). Data on the right originate from OSTIA satellite and in situ data (SST) and surface drifter climatology by Lumpkin and Johnson (2013). Figure adapted from Vic et al. (2014). White rectangles depict the model domain used for the 1/2°-resolution model of the Arabian Sea.

Seasonal coastal upwelling and downwelling is observed in the velocity and temperature variables at the western boundary. Especially in summer, during the SWM, when the wind stress forcing reaches its maximal values, upwelling is indicated by several variables. The surface zonal velocity is directed eastward, i.e. away from the coast, the global SST minimum occurs during that time period and vertical velocities at the coast are directed upwards. However, given the low resolution of the coastal upwelling (or downwelling) region, the resolved

processes are coarse. The model should be re-run with higher resolution in order to analyse the western boundary upwelling region in the Arabian Sea.

5 Conclusion

The climatological 1/2°-resolution model of the Arabian Sea presents the main circulation features and represents the prominent seasonal upwelling on its Western part. However, the low resolution, with a grid spacing of ~ 60 km prevents the study of smaller scale processes, such as filaments or eddies. Moreover, the main upwelling zone is only as wide as a few grid cells, which renders the analysis of the upwelling coarse. Increasing the model resolution is therefore a future project.

Further foreseen changes of the model include to extend it by unmasking the Persian Gulf and Gulf of Oman, as well as to extend the model domain further south. Setting the domain's southern boundary at the equator or even farther should increase it sufficiently for the potential resolution of the Great Whirl observed by Vic et al. (2014) at approximately 7°N off the coast of Somalia during SWM. The remaining question is whether the Great Whirl can be represented by this 1/2°-resolution model.

References

Arakawa, A. and Lamb, V. R. (1977). Computational design of the basic dynamical processes of the ucla general circulation model. *General circulation models of the atmosphere*, 17:173–265.

Doglioli, A. M. (2016). Modélisation de la circulation océanique. *Notes de Cours et Travaux Dirigés*, pages 1–108.

Large, W. G., McWilliams, J. C., and Doney, S. C. (1994). Oceanic vertical mixing: A review and a model with a nonlocal boundary layer parameterization. *Reviews of Geophysics*, 32(4):363–403.

Lee, C. M., Jones, B. H., Brink, K. H., and Fischer, A. S. (2000). The upper-ocean response to monsoonal forcing in the arabian sea: seasonal and spatial variability. *Deep Sea Research Part II: Topical Studies in Oceanography*, 47(7-8):1177–1226.

Lumpkin, R. and Johnson, G. C. (2013). Global ocean surface velocities from drifters: Mean, variance, el niño–southern oscillation response, and seasonal cycle. *Journal of Geophysical Research: Oceans*, 118(6):2992–3006.

Luther, M. E. and O'Brien, J. J. (1985). A model of the seasonal circulation in the arabian sea forced by observed winds. *Progress in Oceanography*, 14:353–385.

Penven, P., Debreu, L., Marchesiello, P., and McWilliams, J. C. (2006). Evaluation and application of the roms 1-way embedding procedure to the central california upwelling system. *Ocean Modelling*, 12(1-2):157–187.

Penven, P., Marchesiello, P., Debreu, L., and Lefèvre, J. (2008). Software tools for pre-and post-processing of oceanic regional simulations. *Environmental Modelling & Software*, 23(5):660–662.

Shchepetkin, A. F. and McWilliams, J. C. (2005). The regional oceanic modeling system (roms): a split-explicit, free-surface, topography-following-coordinate oceanic model. *Ocean modelling*, 9(4):347–404.

Vic, C., Roullet, G., Carton, X., and Capet, X. (2014). Mesoscale dynamics in the arabian sea and a focus on the great whirl life cycle: A numerical investigation using roms. *Journal of Geophysical Research: Oceans*, 119(9):6422–6443.